AALBORG UNIVERSITY

DENMARK

Modeling and Operation of a HT-PEMFC-based micro-CHP system in LabVIEW

Arsalis, Alexandros

[Link to publication from Aalborg University](#)

Modeling and Operation of a HT-PEMFC-based micro-CHP system in LabVIEW

7th February 2010

(Updated: 23th April 2010)

Documentation

Alexandros Arsalis

Dept. of Energy Technology

Aalborg University

Table of Contents

1 Introduction

1.1 Fuel Cell-based micro-CHP Systems

Fuel cell-based stationary power generation offers a great market opportunity, because the fuel cell technology is capable of achieving higher efficiency, with lower emissions as compared to conventional power systems.

Residential fuel cell systems can be grid-interconnected to allow power flow from/to the grid as needed. This design offers greater flexibility than a stand-alone system, and is very attractive if the incoming power is produced by renewable energy sources, such as wind power. This means that when cheap wind power can be produced, the fuel cell system can operate at a minimum load and therefore reduce the fuel consumption. A fuel cell-based micro-CHP (Combined-Heat-and-Power) system converts on-site the chemical energy in a fuel, e.g. natural gas, into electrical power and heat, as required by the household demand (0.5-5.0 kW_e, 2-10 kW_{th}). If a fossil fuel will be used, a fuel processing unit must be coupled with the fuel cell stack, to allow conversion to hydrogen. Several Balance-Of-Plant (BOP) components are needed for the controlling and smooth operation of the system, while heat exchangers are necessary for the thermal management of the system.

A HT-PEMFC (High Temperature-Proton Exchanger Membrane Fuel Cell) uses a PBI (Polybenzimidazole) membrane, operating at temperatures between 160^oC-200^oC. A HT-PEMFC is therefore an ideal match for a micro-CHP system, because not only the rates of electrochemical kinetics are enhanced and water management and cooling is simplified, but also useful waste heat can be recovered, and lower quality reformed hydrogen may be used as fuel (Zhang & Xie, 2006). Thereby, a simple and compact design, with great reliability in load changes can be accomplished, which is vital for this type of application.

1.2 The Danish micro-CHP Project

The Danish micro-CHP project runs from 2006 to 2012, and includes fuel cell systems based on three different technologies: LT-PEMFC, HT-PEMFC and SOFC. The project is divided into three phases, and two fuel types are used: hydrogen and natural gas. The choice of fuel depends on the fuel cell technology and its availability at the installation sites.

1.2.1 Assumptions

The overall conclusion, concerning the control of the units, is that it should be a combination of electricity- and heat-following strategies. In other words, the electrical load must be fulfilled, but also the design should secure the right amount of heat will be available on demand for the space heating and hot water

loads. In connection to this and to enable greater operational flexibility, the system is connected to the grid and also it includes a heat storage system (e.g. a stratified 350L water tank, operating at an average temperature of around $65^{\circ}C$). Further on, an auxiliary burner for peak production of thermal energy is under consideration to be integrated to the end-user system (Pedersen & Balslev, 2009).

The HT-PEMFC-based micro-CHP units are developed by Dantherm Power and operate on natural gas. Experimental tests, with pure hydrogen fuel, showed start-up times of 30-60 minutes, with an electrical efficiency of 40-58% (LHV-based). From the operating point of the finalized design, an efficiency of 50% is expected. Further experimental tests and calculations showed a potential system efficiency of 85-90% (LHV-based). A fast adaption to load variations was also observed.

1.2.2 Schedule

Phase 1: 2006 - 2007

In the first phase, Danish Micro Combined Heat and Power developed micro combined heat and power unit prototypes with PEM and SOFC fuel cells. These prototypes were tested by DGC (Danish Gas Technology Centre).

Phase 2: 2007 - 2010

In the second phase ten micro combined heat and power units will be installed and tested at the homes of selected consumers in Lolland and Sønderborg Municipalities. In Lolland, a hydrogen mini grid will be installed to supply the units with hydrogen. The units will be continuously improved on the basis of test results.

Phase 3: 2010 - 2012

In the third phase, micro combined heat and power units will be installed and demonstrated at the homes of around 100 consumers in the two municipalities. This will allow Danish Micro Combined Heat and Power to gather and analyse experiences related to installation, operation, maintenance and user satisfaction that will be used for further improvements of the units and the training of engineers

1.2.3 Results

Results from phase 1

In phase 1, Topsøe Fuel Cell developed Denmark's first SOFC fuel cells for micro combined heat and power units on natural gas. IRD developed prototypes of micro combined heat and power units with PEM fuel cells on hydrogen. Dantherm developed prototypes based on Topsøe's fuel cell stacks in micro combined heat and power units and also tested the use of foreign PEM cells. Danfoss developed the micro combined heat

and power units' heat storage and a converter from direct current to alternating current. All micro combined heat and power unit prototypes have been tested by DGC. The actual test results can be downloaded here.

Results from phase 2

In phase 2, Danish Micro Combined Heat and Power will obtain the first experiences from Lolland and Sønderborg Municipalities where 10 micro-CHP units will be installed at the homes of selected consumers. Results from Danish Micro Combined Heat and Power's phases will be shown on this page (micro-CHP, 2010).

1.3 Project Objectives

The proposed micro-CHP system, shown in Figure 1, is modeled in LabVIEW (see Appendix) to allow easiness in user usage of the program, and to allow future experimental testing capabilities with Data Acquisition hardware. The project's objectives are the following:

1. Design of a system at nominal load to investigate operating behavior and geometric analysis of the most important system components.
2. Model in detail all necessary components/subsystems, with emphasis on the fuel processing system, to allow a realistic analysis of the system's parameters.
3. Apply an averaged load profile for a single Danish household on the proposed system. The load profile must include all necessary residential loads (electrical, hot water and space heating).
4. Operate the system at part-load to investigate the system's behavior at off-design conditions, and the effects of an electricity-led operation on the total heat-load.
5. Validate the proposed system, with relevant references from the literature, to investigate its validity. Analyze all possible sources of discrepancy.
6. Extract conclusions on the proposed system potential, in terms of modeling with LabVIEW and future experimental testing using the modeled system as a basis.

In connection to the above objectives, the following models were designed individually and then coupled together to create the overall system:

- HT-PEMFC Stack;
- Steam Methane Reformer (SMR) Reactor;
- Water Gas Shift (WGS) Reactor;
- Plate Heat Exchangers;
- By-pass Valves;

- Mixers;

- Steam Generator;

- Combustor;

- Water Pump.

The other components shown in Figure 1 are not modeled individually, but assumptions and calculations (included in the individual models described above) have been made to include their effect in the overall system. These components are the following:

- Condenser/Water knock-out device;

- Desulfurizer;

- Fan (combustor);

- Air Blower.

1.4   Residential Load Requirements

In order to synthesize and design the proposed micro-CHP system, the energy requirements for a representative residential building must be established. For the current research study, the representative residential building is a typical Danish single-family household (130m^2 house with four persons: two adults and two children). A micro-CHP unit of approximately 1kW$_e$ can be used, if a heating-base load strategy is utilized. (de Wit, 2006). The types of residential loads considered are the following:

(a) Electrical load;

(b) Space heating load;

(c) Hot water load.

Averaged daily power load curves for all three loads were measured for 25 houses in 1991 at a 15 minute average time segment. For the purposes of this research study, the entire load profile has been simplified into three time segments, i.e. winter, summer, and spring (autumn) (Korsgaard, Nielsen, & Kær, 2008).

Table 1. Mean residential load requirements for a typical Danish household.

Residential Load Type	Time Segment					
	Winter		Summer		Spring	
	Mean	Max	Mean	Max	Mean	Max
Electrical Load (W$_e$)	540	950	380	650	460	920
Space Heating Load (W$_{th}$)	1450	1930	70	140	600	1070
Hot Water Load (W$_{th}$)	330	1080	230	1420	310	1620

It is clear from Table 1 that the winter segment appears to be the one with the most stringent residential loads. Therefore the system must be designed to fulfill the maximum winter electrical load $\left(0.95\text{kW}_e\right)$, since the proposed micro-CHP system assumes an electricity-led operation. It should be noted that at short time segments the electrical power demand will exceed 1kW_e.

On the other hand, the remaining heat load demand can be satisfied with external means, e.g. auxiliary burner. It should be noted that this is beyond the scope of the project, and only the percentage of heating load fulfilled from the proposed system will be analyzed.
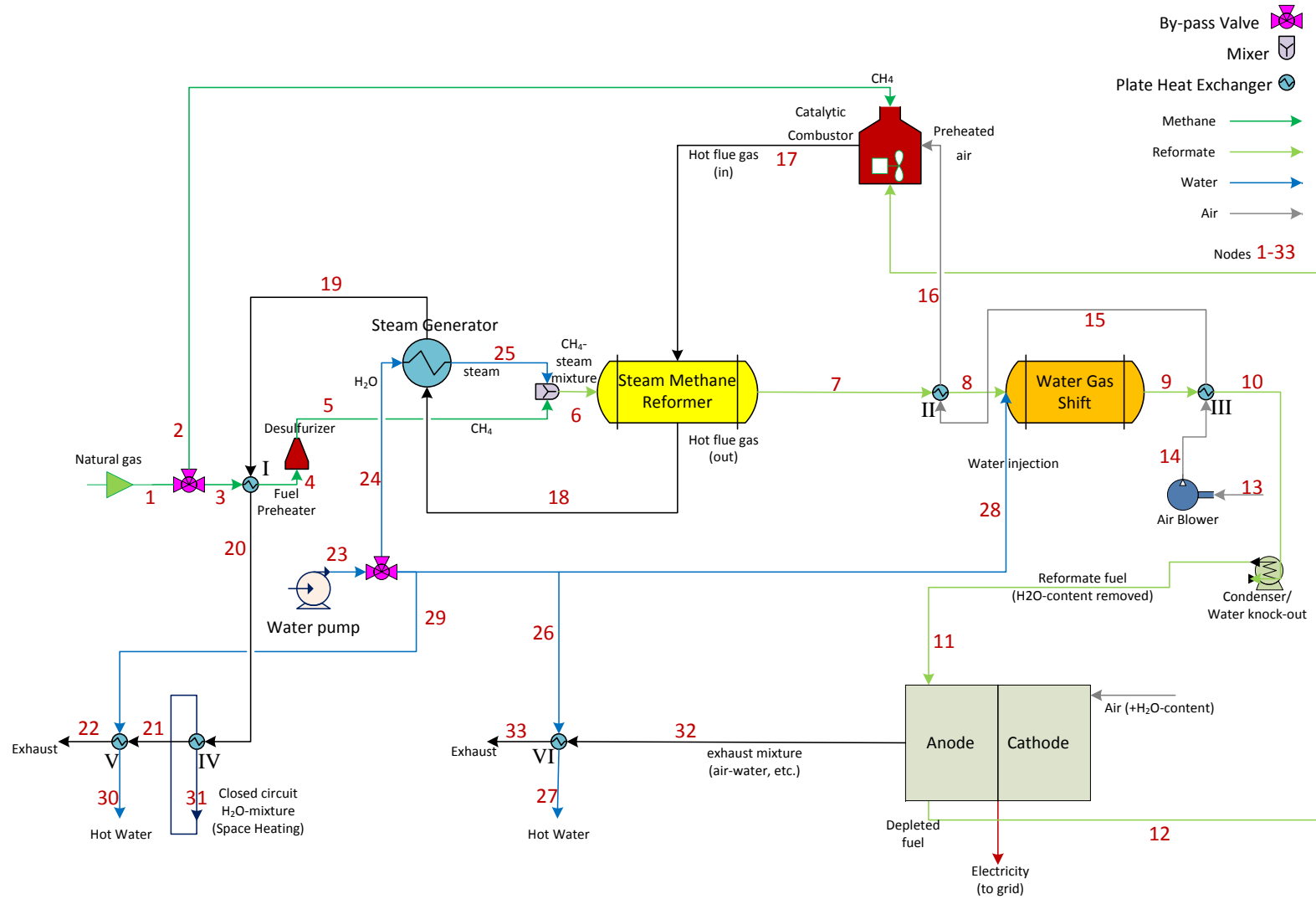
Figure 1. Schematic of the proposed micro-CHP system.

2   HT-PEMFC-based micro-CHP System: Configurations and Models

All the individual models are described in the following sections in terms of input and output parameters, and mathematical modeling equations. Specific assumptions for the particular model under study are also given. The overall assumptions are given below:

- The overall system is assumed to produce a nominal net power output of $1kW_e$.
- The system is considering only an electricity-led operation[1], where the thermal power production for the other residential needs (hot water & space heating) will be calculated according to the heat produced as a by-product of the electrical power production.

2.1   Description of the Operating Principle

Methane (for the purpose of modeling simplicity natural gas is assumed to behave as methane) is desulfurized at an acceptable level. Water is pumped from the line in the steam generator, where is superheated with flue gas exhausted by the shell-side of the SMR reactor. Superheated steam and preheated natural gas are mixed in a mixer, and then the steam-fuel mixture is fed to the tube-side of the SMR reactor. The catalytic combustor's inputs are air, methane (necessary at start-up), and reformate fuel (depleted fuel from the anode of the fuel cell stack). Its main purpose is to provide heat for the endothermic steam methane reforming reaction.

In the SMR reactor, the reforming reaction takes place. It should be noted that the SMR process is based on reaction kinetics, and is modeled as a plug flow reactor with the presence of a catalyst, with experimental data taken from (Xu & Froment, 1989). In terms of heat exchanging, the SMR is modeled as a shell-and-tube heat exchanger, where the shell part carries the hot flue gas, and the tube part carries the vaporized methane-water mixture. The produced hydrogen-rich synthesis gas is mixed with water and enters the water gas shift (WGS) reactor, which is modeled similarly to the SMR. It serves as a reduction of the carbon monoxide content, which is converted to carbon dioxide, into a tolerable level for the fuel cell stack. It also contributes in further hydrogen production.

The reformate fuel enters the anode side of the fuel cell stack, where a part of it is depleted and used in the combustor for the SMR reaction described above. In the cathode of the fuel cell stack, air enters and used for the well-known fuel cell reaction converting the chemical energy of reformate and air into electricity. A

---

[1] Electricity-led operation is defined as dispatching the unit with the intention of meeting as much of the onsite electrical load as possible whilst simultaneously attempting to minimize the amount of electricity exported to the grid.

by-product of this reaction is the hot mixture, which exits from the fuel cell stack. This mixture is used in a plate heat exchanger to satisfy a part of the residential heat load. A part of the residential heat load is also satisfied by the exhausted flue gas at the natural gas pre-heater; Flue-gas is then passed through open-loop and closed-loop heat exchangers for water heating and space heating, respectively.

2.2 HT-PEM Fuel Cell Stack

The HT-PEMFC stack model is based on (Korsgaard, Nielsen, & Kær, 2008). Initially, the model calculates the required hydrogen feed based on the number of cells specified in the model. This will be the value of the full-load feed fuel, which can become a constant and the basis for the part-load calculations, where the model has been modified to have the feed reformate fuel (hydrogen-rich gas) as an input to the model, in order to allow the calculation of power output at part-load conditions. Similarly the current density is constant at full-load $\left(0.2\,cm^2/A \right)$ and a calculated variable at part-load conditions.

The fuel cell stack is based on the following assumptions:

- A single fuel cell stack is considered, although a more realistic model could utilize a number of interconnected stacks.

- The model considers only the reaction of hydrogen with oxygen (air). All other substances are considered inactive.

- The reformate fuel after the WGS Reactor/Plate Heat Exchanger stage passes through a condenser/knock-out stage, where all the water content in the fuel is removed. It should be noted that this assumption is not appropriate in a realistic system (because the fuel cell stack membranes would be dried), but it has been used to simplify the calculations. But, some water-content it is still present because the moisture content in the incoming air is still used in the calculations.

- The temperature of the reformate fuel incoming the fuel cell anode is 160 degC, which is the fuel cell stack operating temperature.

- Heat losses are not considered in the calculations.

Table 2.   Constants used in the HT-PEM fuel cell stack model.

	Variable Description	Model Equation			Variable Description	Model Equation
F	Faraday's Number	$96485\,\dfrac{C}{mol}$		i	Current density	Assigned Value
R	Ideal Gas Constant (molar)	$8.314\,\dfrac{J}{K\,mol}$		p	Operating Pressure	$1\,bar$
LHV_{CH_4}	Lower Heating Value	$5.0056\mathrm{E}+07\,\dfrac{J}{kg}$		λ_i	Stoichiometry of species i	Assigned Value
LHV_{H_2}	Lower Heating Value	$1.1986\mathrm{E}+08\,\dfrac{J}{kg}$		$r_{ambient}$	Ambient Relative Humidity	0.7

$T_{ambient}$	Ambient Temperature	$20\ ^oC$	A_{cell}	Cell Active Area	$49\ cm^2$
T_{cell}	Operating Temperature	$160\ ^oC$	n_{cells}	Number of cells	Assigned Value

Table 3. HT-PEM fuel cell stack model.

Variable Description		Model Equation
x_i	Mole fraction of species i	$x_i = \dfrac{\dot{n}_i}{\dot{n}_{total}}$
y_i	Mass fraction of species i	$y_i = \dfrac{\dot{m}_i}{\dot{m}_{total}}$
b_{fh}	H_2 desorption rate	$b_{fh,o} = 2.038E-6 \quad E_{bfh} = 47904 \quad b_{fh} = b_{fh,o}\exp\left(\dfrac{-E_{bfh}}{RT_{cell}}\right)$
k_{ec}	CO electro-oxidation rate	$k_{ec,o} = 3.267E18 \quad E_{kec} = 196829 \quad k_{ec} = k_{ec,o}\exp\left(\dfrac{-E_{kec}}{RT_{cell}}\right)$
k_{eh}	H_2 electro-oxidation rate	$k_{eh,o} = 25607 \quad E_{keh} = 34777 \quad k_{eh} = k_{eh,o}\exp\left(\dfrac{-E_{keh}}{RT_{cell}}\right)$
k_{fc}	CO adsorption rate	$k_{fc,o} = 94.08 \quad E_{kfc} = 19045 \quad k_{fc} = k_{fc,o}\exp\left(\dfrac{-E_{kfc}}{RT_{cell}}\right)$
k_{fh}	H_2 adsorption rate	$k_{fh,o} = 2.743E24 \quad E_{kfh} = 189900 \quad k_{fh} = k_{fh,o}\exp\left(\dfrac{-E_{kfh}}{RT_{cell}}\right)$
V_0	Voltage	$0.95\ V$
i_0	Current density	$33323\exp\left(-0.04368 T_{cell}\right)$
$\alpha_{cathode}$	Cathode overpotential transfer coefficient	$\alpha_{cathode} = \left(-1.891 + 0.005522 T_{cell}\right)0.5$
α_{anode}	Anode overpotential transfer coefficient	$\alpha_{anode} = 0.5$
R_{ohmic}	Ohmic resistance	$R_{ohmic} = -0.0001667 T_{cell} + 0.2289$
R_{diff}	Diffusion resistance	$R_{diff} = 0.4306 - 0.0008203 T_{cell}$
η_a	Anode overpotential	$\eta_a = \dfrac{RT_{cell}}{\alpha_{anode}F}\mathrm{arcsinh}\left(\dfrac{i}{2k_{eh}\theta_{H_2}}\right)$
η_c	Cathode overpotential	$\eta_c = \dfrac{RT_{cell}}{4\alpha_{cathode}F}\ln\left(\dfrac{i_0+i}{i_0}\right) + R_{diff}\left(\dfrac{i}{\lambda_{air}-1}\right)$
η_{ohmic}	Ohmic losses	$\eta_{ohmic} = iR_{ohmic}$
V_{cell}	Total cell voltage	$V_{cell} = V_0 - \eta_a - \eta_c - \eta_{ohmic}$
W_{cell}	Power density	$W_{cell} = V_{cell}i$
V_{stack}	Stack voltage	$V_{stack} = V_{cell}n_{cells}$
P_{stack}	Fuel cell stack electrical power output	$P_{stack} = A_{cell}n_{cells}W_{cell}$
I_{stack}	Current	$I_{stack} = \dfrac{P_{stack}}{V_{stack}}$
$\dot{m}_{H_2,in}$	Inlet flow rate of H_2	$\dot{m}_{H_2,in} = \lambda_{H_2}\dfrac{M_{H_2}P_{stack}}{2V_{cell}F}$
$\dot{m}_{H_2,out}$	Outlet flow rate of H_2	$\dot{m}_{H_2,out} = \dot{m}_{H_2,in}\left(\lambda_{H_2}-1\right)$
$\dot{m}_{air,in}$	Inlet flow rate of air to the fuel cell stack	$\dot{m}_{air,in} = \lambda_{air}\dfrac{M_{air}P_{stack}}{0.21(4)V_{cell}F}$
$\dot{m}_{O_2,used}$	Oxygen consumed in the fuel cell stack	$\dot{m}_{O_2,used} = \dfrac{M_{O_2}P_{stack}}{4V_{cell}F}$
$\dot{m}_{air,out}$	Outlet air flow from the fuel cell stack	$\dot{m}_{air,out} = \dot{m}_{air,in} - \dot{m}_{O_2,used}$
$\dot{m}_{H_2O,ambient}$	Inlet water flow rate resulting from water content in the ambient air	$\dot{m}_{H_2O,ambient} = \dot{m}_{air,in}\omega_{ambient}$
$\dot{m}_{water,production}$	Outlet water flow rate produced in the fuel cell stack	$\dot{m}_{water,production} = \dfrac{M_{H_2O}P_{stack}}{2V_{cell}F}$

$\dot{m}_{water,out}$	Total outlet water flow rate exiting from the fuel cell stack	$\dot{m}_{water,out} = \dot{m}_{water,production} + \dot{m}_{H_2O,ambient}$
$\left(\dot{m}_{total,fc}\right)_{out}$	Total outlet flow rate exiting from the fuel cell stack	$\left(\dot{m}_{total,fc}\right)_{out} = \dot{m}_{water,out} + \dot{m}_{air,out}$
$\eta_{el,HHV}$	Fuel cell stack electrical efficiency based on HHV	$\eta_{el,HHV} = \dfrac{P_{stack}}{\dot{m}_{fuel}HHV_{fuel}}$
$\eta_{el,LHV}$	Fuel cell stack electrical efficiency based on LHV	$\eta_{el,LHV} = \dfrac{P_{stack}}{\dot{m}_{fuel}LHV_{fuel}}$
ΔH	Heat of formation	$\Delta H = h_{f,H_2O} - \left(\dfrac{1}{2}h_{f,O_2} + h_{f,H_2}\right)$
ΔG	Gibbs free energy	$\Delta G = \Delta H - T\Delta S$
ΔS	Entropy difference	$\Delta S = s_{f,H_2O} - \left(\dfrac{1}{2}s_{f,O_2} + s_{f,H_2}\right)$
E_{th}	Theoretical voltage	$E_{th} = \dfrac{-\Delta G}{nF}$

2.3 Steam Methane Reformer (SMR) Reactor

The kinetic and geometric model of the SMR reactor is described analytically in Table 4. The following assumptions were made for the SMR Reactor:

- The reaction kinetics are based on the generalized Langmuir-Hinshelwood kinetic model by (Xu & Froment, 1989).
- The model considers a steady-state non-isothermal plug flow reactor (PFR).
- There is a presence of catalytic material in a packed bed reactor (PBR) arrangement.
- Only three chemical kinetic reactions are assumed active.
- The SMR reactor is heat integrated (shown in Figure 2) with a shell-and-tube heat exchanger design. The reformate fuel flows through the tube side, while the hot flue flows through the shell side. In other words, the endothermic reaction is accomplished with heating from an external source (combustor).
- The external shell-side wall is considered adiabatic.
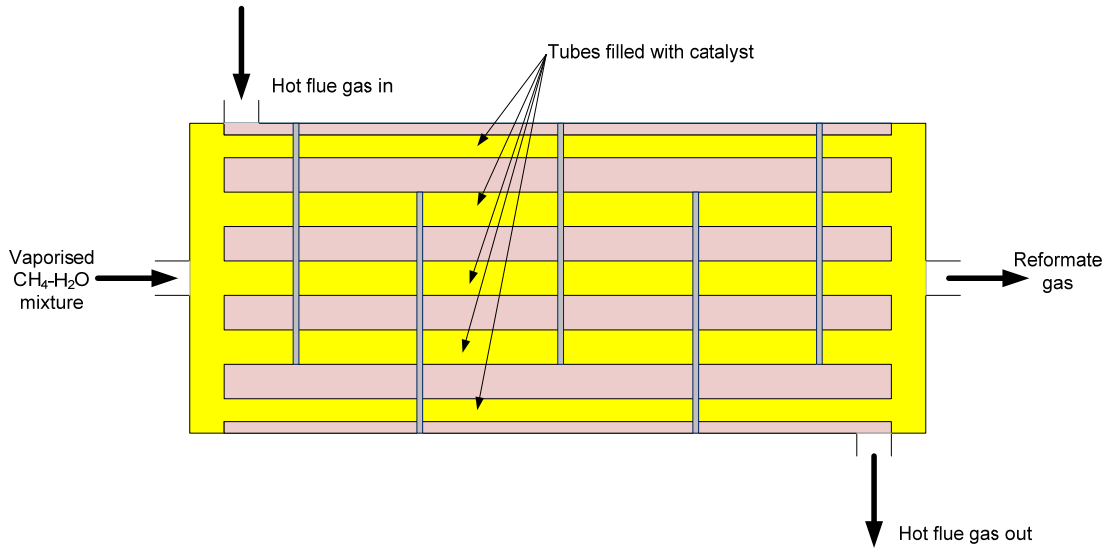
Figure 2. Schematic of the steam methane reformer (modelled as a shell-and-tube heat exchanger – packed-bed reactor).

2.3.1 Chemical Kinetics

Reaction kinetics data are necessary for the configuration and sizing of the reactor and they are obtained from laboratory experiments. For catalyzed reactions the Langmuir-Hinshelwood kinetic equation is found to fit the experimental kinetic data more accurately than the power-law expression (Nielsen, 2005):

- The *denominator* describes the concentrations of reactants & products strongly absorbed on the catalyst;
- The *prefix η* describes the overall effectiveness factor, which accounts for mass and heat transfer resistances (both internal & external) to the catalyst particles.

For the fuel processing under study only the following reactions are considered:

$$CH_4 + H_2O \rightleftharpoons CO + 3H_2 \qquad\qquad \Delta H_{298} = 206.2\, kJ/mol \qquad\qquad (1)$$

$$CO + H_2O \rightleftharpoons CO_2 + H_2 \qquad\qquad \Delta H_{298} = -41.1\, kJ/mol \qquad\qquad (2)$$

$$CH_4 + 2H_2O \rightleftharpoons CO_2 + 4H_2 \qquad\qquad \Delta H_{298} = 164.9\, kJ/mol \qquad\qquad (3)$$
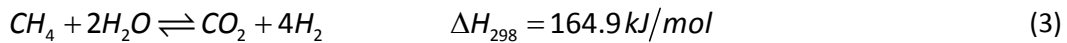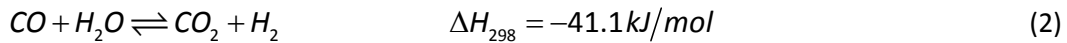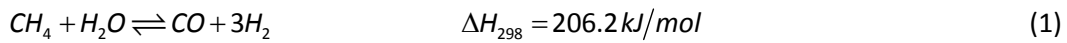
Table 4.   Kinetic and geometric model of the SMR reactor.

Variable Description		Model Equation
T_0	Inlet Temperature (K)	Assigned Value
p_0	Inlet Pressure (bar)	Assigned Value
k_{n_a}	Rate Parameters	$k_{1_a} = A_{k_1} \exp\left(-E_{k_1} \dfrac{1}{R_u T}\right) \qquad k_{2_a} = A_{k_2} \exp\left(-E_{k_2} \dfrac{1}{R_u T}\right) \qquad k_{3_a} = A_{k_3} \exp\left(-E_{k_3} \dfrac{1}{R_u T}\right)$

K_n	Equilibrium constants	$K_1 = 1.026676 \exp\left(\dfrac{-26830}{T} + 30.11\right)$ $\quad K_2 = \exp\left(\dfrac{4400}{T} - 4.063\right)$ $\quad K_3 = K_1 K_2$
K_i	Adsorption equilibrium parameters	$K_{CO} = A_{K_{CO}} \exp\left(-dH_{K_{CO}} \dfrac{1}{R_u T}\right) \qquad K_{H_2} = A_{K_{H_2}} \exp\left(-dH_{K_{H_2}} \dfrac{1}{R_u T}\right)$ $K_{CH_4} = A_{K_{CH_4}} \exp\left(-dH_{K_{CH_4}} \dfrac{1}{R_u T}\right) \qquad K_{H_2O} = A_{K_{H_2O}} \exp\left(-dH_{K_{H_2O}} \dfrac{1}{R_u T}\right)$
D_i	Inlet Diameter (m)	Assigned value
D_o	Outlet Diameter (m)	Assigned value
ω	Cross-sectional area (m^2)	$\omega = \dfrac{\pi D_i^2}{4}$
L_{tube}	Tube length (m)	Assigned value
p_i	Partial pressures (bar)	$p_{H_2O} = p \dfrac{F_{H_2O,o} - F_{CH_4,o}\left(x_{CH_4} + x_{CO_2}\right)}{F_{total,o} + 2F_{CH_4,o}x_{CH_4}} \qquad p_{CH_4} = p \dfrac{F_{CH_4,o}\left(1 - x_{CH_4}\right)}{F_{total,o} + 2F_{CH_4,o}x_{CH_4}}$ $p_{N_2} = p \dfrac{F_{N_2,o}}{F_{total,o} + 2F_{CH_4,o}x_{CH_4}} \qquad p_{CO_2} = p \dfrac{F_{CO_2,o} + F_{CH_4,o}x_{CO_2}}{F_{total,o} + 2F_{CH_4,o}x_{CH_4}}$ $p_{H_2} = p \dfrac{F_{H_2,o} + F_{CH_4,o}\left(3x_{CH_4} + x_{CO_2}\right)}{F_{total,o} + 2F_{CH_4,o}x_{CH_4}} \qquad p_{CO} = p \dfrac{F_{CH_4,o}\left(x_{CH_4} - x_{CO_2}\right)}{F_{total,o} + 2F_{CH_4,o}x_{CH_4}}$
u_s	Superficial velocity (m/s)	$u_s = u_{s0} \dfrac{p_0}{p} \dfrac{T}{T_0} \dfrac{F_{total,o} + 2F_{CH_4,o}x_{CH_4}}{F_{total,o}}$

2.3.2 Heat Transfer

The heat transfer model is based on (Kim, 2008), where the shell-and-tube heat integration model is based on a transient model. For the current research study, the model was simplified in a steady-state one, where the partial differential equations are simplified into ordinary differential equations (Table 5). The convective heat transfer coefficient of the inside tube wall is based on a semi-empirical relation for spherical packing (Li & Finlayson, 1977).

Table 5. Heat transfer model of the shell-and-tube SMR reactor.

	Variable Description	Model Equation
n_{shells}	Number of shells	Assigned value
n_{tubes}	Number of tubes	Assigned value
k_{ref}	Thermal conductivity of the reformate gas	Assigned value
d_p	Catalyst diameter	Assigned value
Re_p	Reynolds number	Assigned value
h_w	Tube-side heat transfer coefficient	$h_w = 2.03 Re_p^{0.8} \dfrac{k_{ref}}{D_i} \exp\left(-\dfrac{6 d_p}{D_i}\right)$
h_s	Shell-side heat transfer coefficient	$h_s = 0.36 \left(\dfrac{k_s}{D_{eq}}\right)\left(\dfrac{D_{eq} G_s}{\mu_s}\right)^{0.55}\left(\dfrac{C_{p,s}\mu_s}{k_s}\right)^{1/3}\left(\dfrac{\mu_s}{\mu_{wall}}\right)^{0.14}$
$\dfrac{dT_s}{dz}$	Flue gas temperature gradient	$\dfrac{dT_s}{dz} = \dfrac{\pi h_s D_o\left(T_w - T_s\right)}{\dot{m}_s C_{p,s}}$
T_w	Inside tube wall temperature	$T_w = \dfrac{D_o h_s T_s + D_i h_w T}{D_o h_s + D_i h_w}$

2.4   Water Gas Shift (WGS) Reactor

The main assumptions for the WGS reactor are the following:

- The inlet composition for the WGS reactor is the sum of the exit composition of the SMR reactor and the injected water;

- The heat exchanger prior to entering the WGS reactor cools the WGS inlet temperature to an appropriate level needed by the WGS reactor;

- The CO content, in terms of molar composition, should be reduced to an acceptable level of 0.1% – 0.2%;

- The kinetic constant (using a power law relationship) is at steady state (Keiski, Salmi, Niemisto, Ainassaari, & Pohjola, 1996).

2.4.1   Chemical Kinetics

The kinetic model of the WGS reactor is described in Table 6. The water gas shift reaction is the following:

$$CO + H2O \rightleftharpoons CO2 + H2 \qquad\qquad (4)$$

Table 6.   Kinetic model of the WGS reactor.

Variable Description		Model Equation
$\dot{n}_{total,o}$	Inlet molar flow rate	$\dot{n}_{total,o} = \dot{n}_{H_2O,i} + \dot{n}_{CH_4,i} + \dot{n}_{N_2,i} + \dot{n}_{CO_2,i} + \dot{n}_{H_2,i} + \dot{n}_{CO,i} + \dot{n}_{O_2,i}$
$dH_{r,1}$	Enthalpy of reaction (polynomial curve fit)	$dH_{r,1} = -35.5193858 - 0.0369753562T + 0.0000813400667T^2 - 6.92910551^{-8}T^3$
K_T	Equilibrium constant (Davies & Lihou, 1971)	$K_T = \exp\left(\dfrac{4400}{T} - 4.063\right)$
K_{WGS}	Kinetic power law fit parameters (Keiski, 1996)	$K_{WGS} = k_0 \exp\left(\dfrac{-E_a}{R_u T}\right)$
r_{CO}	Reaction rate (Keiski, 1996)	$\beta = \dfrac{C_{CO_2} C_{H_2}}{K_T C_{CO} C_{H_2O}}$ $r_{CO} = K_{WGS} C_{CO}{}^n C_{H_2O}{}^m C_{CO_2}{}^{p_1} C_{H_2}{}^q (1 - \beta)$
ρ_g	Gas density assuming ideal gas	$\rho_g = \dfrac{M_{H_2O}p_{H_2O} + M_{CH4}p_{CH4} + M_{N2}p_{N2} + M_{CO2}p_{CO2} + M_{H2}p_{H2} + M_{CO}p_{CO} + M_{O2}p_{O2}}{\dfrac{R_u}{T}}$
μ	Molar average mixture viscosity	$\mu = \dfrac{p_{CH_4}\mu_{CH_4} + p_{N_2}\mu_{N_2} + p_{CO_2}\mu_{CO_2} + p_{H_2O}\mu_{H_2O} + p_{CO}\mu_{CO} + p_{H_2}\mu_{H_2} + p_{O_2}\mu_{O_2}}{p}$
$\dfrac{dx_{CO}}{dz}$	CO extent of reaction	$\dfrac{dx_{CO}}{dz} = \omega\rho_{wiremesh}\dfrac{3600 r_{CO}}{\dot{n}_{CO,i}}$
$\dfrac{dT}{dz}$	Temperature gradient	$\dfrac{dT}{dz} = \dfrac{\rho_{wiremesh}}{\rho_g c_{p,mass} u_s}\left(-r_{CO} dH_{r,1}\right)$

2.5   Plate Heat Exchangers

In the current configuration four heat exchangers of the plate type are used. All flows are unmixed. The main advantage of a plate heat exchanger is its compactness. These heat exchangers fulfill the following system needs:

- Fuel pre-heater: Flue gas, exhausted from the steam generator's flue gas side, preheats the natural gas, before being mixed with the superheated steam in the mixer.

- Water heater: The exhaust water mixture produced from the fuel cell stack is used to heat tap water at a temperature high enough for domestic use.

- Space heating heater: The exhaust water mixture produced from the fuel cell stack is used to heat the fluid (water mixture) in a closed circuit for space heating.

- High temperature reformate fuel cooler: it is located between the SMR and the WGS reactors to cool the reformate gas exiting the SMR reactor. The reformate gas must reach a lower temperature before entering the WGS reactor. On the cold-side of the heat exchanger, the air absorbs the heat before entering the combustor.

- Low temperature reformate fuel cooler: It is located after the WGS reactor and cools the reformate gas with ambient air. This is necessary to ensure the reformate fuel is at a low temperature before entering the condenser, and subsequently the fuel cell stack. On the cold-side of the heat exchanger the ambient air is heated, and then send to the high temperature reformate fuel cooler for further heating, as explained above.

The modeling calculates the heat transfer rate and the UA-value needed to fulfill the heat exchange for the given mass flow rates and inlet temperatures.

Table 7.   Heat transfer model of the plate heat exchanger.

Variable Description		Model Equation
$T_{h,avg}$	Average hot-side temperature	$T_{h,avg} = \dfrac{T_{h,i} + T_{h,o}}{2}$
$\dot{Q}$	Heat transfer rate	$\dot{Q} = \dot{m}_h C_{p,h}\left(T_{h,i} - T_{h,o}\right) = \dot{m}_c C_{p,c}\left(T_{c,o} - T_{c,i}\right)$
$\Delta T_{lm,CF}$	Logarithmic mean temperature difference	$\Delta T_{lm,CF} = \dfrac{\Delta T_1 - \Delta T_2}{\ln\left(\dfrac{\Delta T_1}{\Delta T_2}\right)}$
UA	UA-value	$UA = \dfrac{\dot{Q}}{\Delta T_{lm,CF}}$

2.6   Mixers & By-pass Valves

The mixers and by-pass valves used in the micro-CHP system are necessary for the operation and the regulation of the system. The modeling of each mixer and by-pass valves is done with simple mass and energy balances, assuming no pressure losses. In the current configuration the following three mixers are used: Superheated steam is mixed with preheated natural gas before entering the SMR reactor.

- The reformate gas exiting from the SMR reactor mixes with water from the water pump.
- A mixer is also used to mix the reformate gas with the depleted fuel (from the fuel stack) for use in the combustor.

In the current configuration the following five by-pass valves are used:

- Three by-pass valves distribute the water pumped by the water pump to the steam generator, the fuel cell stack, and for water injection in the reformate gas.
- A by-pass valve after the natural gas line inlet adds fuel to the combustor, as needed.
- Finally, a by-pass valve splits the reformate fuel exiting the WGS reactor to the condenser and to the combustor, as needed.

2.7   Steam Generator

The steam generator model is based on the modeling assumptions analyzed in section 2.5 for the plate-heat exchanger. The steam generator is divided into three sections: economizer, evaporator, and super-heater (see Figure 3).

In the water/steam side of the SG, water is pumped in the economizer section by the water pump, and undergoes phase changes (as shown in Figure 3) until it becomes superheated steam. The steam is then mixed with preheated fuel (methane) in the mixer, at the same temperature.

In the flue gas side, flue gas exhausted from the SMR reactor is used to heat the water following the reverse path, as compared to the water side. The exhausted flue gas is then used to preheat the methane in the fuel preheater (plate heat exchanger).
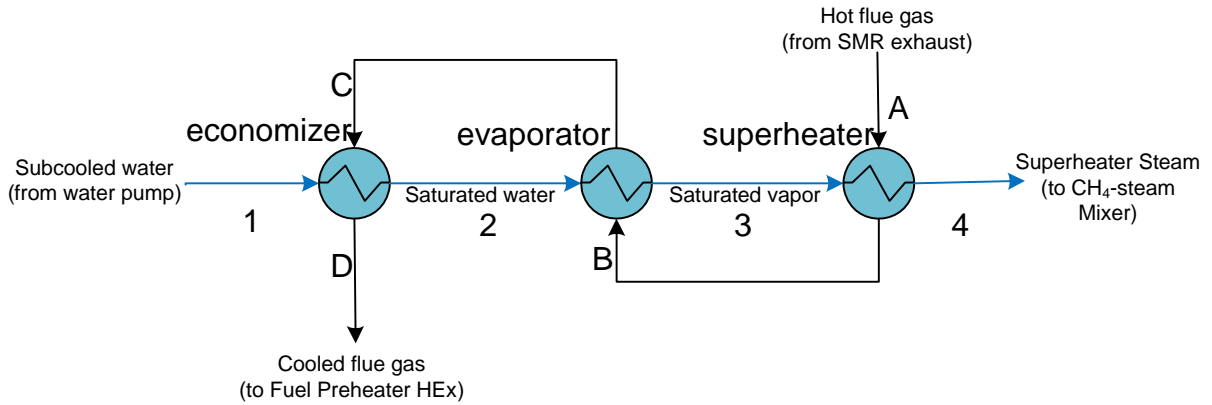
Figure 3. Schematic of the Steam Generator.

2.8 Catalytic Combustor

Although the primary purpose of the catalytic combustor (burner) is to produce heat for the steam reforming reaction in the SMR Reactor, it can be used to produce additional heat to supplement the heat production from the fuel cell stack. In this manner, the residential heat demand can be fulfilled. Depleted fuel (hydrogen-rich gas) from the fuel cell is combusted with air in the catalytic combustor and the following assumptions concerning the operation of the combustor have been made:

1. The flue gas temperature is regulated to remain constant at 1100K. Therefore depending on the amount of the fuel, the amount of air is regulated accordingly. The effect of NOx-content has not been investigated in the current model.

2. The flue gas flow rate is tested whether it is adequate to fulfill the SMR reaction, otherwise more fuel is needed to be combusted. In the latter case, natural gas from the line can be used through the relevant by-pass valve.

3. The air used in the combustor is twice preheated by two plate heat exchangers, before and after the WGS reactor.

The relevant stoichiometric combustion reactions are given below:

$$H_2 + 0.5(O_2 + 3.76N_2) \rightarrow H_2O + 0.5(3.76)N_2 \tag{5}$$

$$CH_4 + 2(O_2 + 3.76N_2) \rightarrow CO_2 + 2H_2O + 7.52N_2 \tag{6}$$
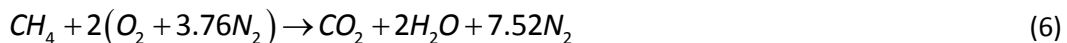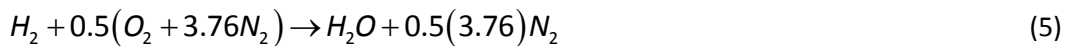
2.9 Water Pump

The water pump is used to pump water to the steam generator, the WGS reactor (water injection), and to the water heater (plate heat exchanger after the fuel cell stack exit). Since the thermodynamic states in the

inlet are known and the outlet thermodynamic states can be fixed as desired, what is left is a calculation of the pump power consumed. The corresponding mass and energy balances are given by:

$$\dot{m}_{in}^{pump} = \dot{m}_{out}^{pump} \tag{7}$$

$$\dot{W}_{pump} = \left[\dot{m}_{in} \left(h_{out} - h_{in} \right) \right]_{pump} \tag{8}$$

where $\dot{m}_{in}$ is the non-pressurized mass flow rate entering the pump, $\dot{m}_{out}$ the pressurized mass flow rate exiting the pump, $\dot{W}_{pump}$ the pump work rate consumption, and h_{in}^{pump}, and h_{out}^{pump} are the corresponding enthalpies for the mass flow.

The pressure boost is around 0.2 bar, assuming that every component has a pressure loss of 0.015 bar. This assumption is done in order to have a fuel cell stack pressure (reformate fuel in the anode) slightly above atmospheric, close to 1.05 bar.

2.10 Overall System Definitions

The overall system total efficiency is defined as the sum of the system thermal power and the net system electrical power, divided by the chemical energy input to the system:

$$\left(\eta_{system} \right)_{total} = \frac{\left(\dot{W}_{electrical} \right)_{net} + \left(\dot{Q}_{thermal} \right)_{total}}{\dot{m}_{CH_4,in} E_{CH_4}} \tag{9}$$

The net system electrical power output efficiency is:

$$\left(\eta_{electrical} \right)_{net} = \frac{\left(\dot{W}_{electrical} \right)_{net}}{\dot{m}_{CH_4,in} E_{CH_4}} \tag{10}$$

where E_{CH_4} can be either the Higher Heating Value $\left(HHV_{CH_4} \right)$ or the Lower Heating Value $\left(LHV_{CH_4} \right)$. The net system electrical power output is calculated by subtracting the power input from the fuel cell stack power output. The power input to the system consists of the power input for the water pump and the air blower. All other power input requirements are considered negligible.

$$\left(\dot{W}_{electrical} \right)_{net} = P_{FCS} - P_{WP} - P_{AB} \tag{11}$$

The total (theoretical) system thermal power efficiency is:

$$\left(\eta_{thermal}\right)_{total} = \frac{\left(\dot{Q}_{thermal}\right)_{total}}{\dot{m}_{CH_4,in}E_{CH_4}} \tag{12}$$

The total thermal power output of the system is the addition of the heat balances in the SMR reactor, the burner, and the fuel cell stack, and subtraction of the net system electrical power output:

$$\left(\dot{Q}_{thermal}\right)_{total} = \dot{Q}_{SMR} + \dot{Q}_{Combustor} + \dot{Q}_{fc,stack} - \left(\dot{W}_{electrical}\right)_{net} \tag{13}$$

2.10.1 Fuel Cell Stack Heat Balance

The heat balance in the fuel cell stack consists of the reformate fuel input to the anode subtracting the depleted fuel to the combustor, the air input to the cathode subtracting the excess nitrogen-oxygen mixture, and then subtracting the water-mixture stack output in the anode:

$$\begin{aligned}\dot{Q}_{fc,stack} = &\dot{m}_{ref.fuel,in}h_{ref.fuel,in} - \dot{m}_{dep.fuel,out}h_{dep.fuel,out} \\ &+ \dot{m}_{air,in}h_{air,in} - \dot{m}_{air,exh}h_{air,exh} - \dot{m}_{water,mix}h_{water,mix}\end{aligned} \tag{14}$$

2.10.2 SMR Reactor Heat Balance

The inputs in the SMR Reactor are the flue gas from the combustor and the reformate fuel from the mixer, where the outputs are the flue gas to the steam generator and reformate to the plate heat exchanger before the WGS reactor:

$$\dot{Q}_{SMR} = \dot{m}_{ref.fuel,in}h_{ref.fuel,in} - \dot{m}_{ref.fuel,out}h_{ref.fuel,out} + \dot{m}_{f.g.,in}h_{f.g.,in} - \dot{m}_{f.g.,out}h_{f.g.,out} \tag{15}$$

2.10.3 Combustor Heat Balance

The inputs in the combustor are the depleted fuel from the fuel cell stack anode and the preheated air from the heat exchanger before the WGS reactor, where the only output is the flue gas fed to the SMR reactor's shell-side:

$$\dot{Q}_{combustor} = \dot{m}_{dep.fuel,in}h_{dep.fuel,in} + \dot{m}_{air,in}h_{air,in} - \dot{m}_{f.g.,out}h_{f.g.,out} \tag{16}$$

2.10.4 Cogeneration

For a more realistic analysis of the proposed micro-CHP system, the above calculations are not so critical because the actual waste heat recovered and used for the residential heat loads should be evaluated. Therefore, the cogeneration thermal efficiency is defined as:

$$\left(\eta_{thermal}\right)_{cogen.} = \frac{\left(\dot{Q}_{HEx}\right)_{cogen.}}{\dot{m}_{CH_4,in}E_{CH_4}} \qquad (17)$$

where $\left(\dot{Q}_{HEx}\right)_{cogen.}$ is the actual waste heat recovered by heat exchangers IV, V, and VI.

Therefore, the cogeneration system efficiency is defined as:

$$\left(\eta_{system}\right)_{cogen.} = \frac{\left(\dot{W}_{electrical}\right)_{net} + \left(\dot{Q}_{HEx}\right)_{cogen.}}{\dot{m}_{CH_4,in}E_{CH_4}} \qquad (18)$$

3   Results and Discussion

The most significant components are validated individually, with reference models/values, to investigate their validity and the amount of defect, as compared to the reference models. Finally, the overall system is compared with (Korsgaard, Nielsen, & Kær, 2008).

The results for the proposed system are given for the nominal (full) load of 1kW. This net value includes the fuel cell stack electrical power output, and the air blower and the water pump input power. The off-design performance results are given next to indicate the system's performance at load changes.

Further on, the percentage of heat load fulfilled by the system, as explained in the adopted load profile in section 1.4, is analyzed.

Finally, the component geometries for the most significant components are given. These components include the fuel cell stack, the SMR reactor and the WGS reactor. Also UA-values are given for the heat exchangers.

3.1   Model Validation

The validation of the SMR reactor, the WGS reactor, the HT-PEMFC stack, and the overall system were compared with reference models from the literature. Before validation is explained, it should be noted that mass balances for every component's input/output were performed; the mass balances verified the validity of the results.

The SMR reactor is based on the computational (EES) model developed by (Nielsen, 2005), which is based on the experimental results by (Xu & Froment, 1989).The WGS reactor is based on the computational (EES) model developed by (Nielsen, 2005), which is based on the experimental results (Keiski, Salmi, Niemisto, Ainassaari, & Pohjola, 1996).The HT-PEMFC Stack is based on the computational (EES) model developed by (Nielsen, 2005). All three individual subsystems (subVIs), showed only minor discrepancies between the reference models and the models under study.

Although an analytical comparison between the research under study and a reference system is not possible, due to significant differences between the current system and the systems in the literature, some values can be compared to investigate validity, and also the sources of discrepancy. The chosen reference system is the HT-PEMFC-based micro-CHP system developed by (Korsgaard, Nielsen, & Kær, 2008). The results are given in Table 8. The most significant differences between the two systems are the following:

1. Different heat integration techniques in the SMR reactor. The reference system considers a simple heat integration model without any consideration of the geometric influence of a realistic system. The research project under study considers a shell-and-tube heat integration model as explained in the preceding sections.

2. Different chemical kinetics modeling in the SMR reactor. The reference system considers a continuous stirred-tank reactor (CSTR), based on chemical equilibrium, where the research project under study considers a PFR, based on reaction kinetics, as explained in the preceding sections.

3. Some other differences in the layout of the system components can be noted as well; a steam generator and fuel preheater are modeled in the current system under study, where a mixture vaporizer was modeled in the reference model. Also different heating/cooling between streams are used (e.g. air coolers, etc.).

Nevertheless of the differences between the two systems, the validation has shown a good agreement of the two models, verifying the validity of the research project in study.

Table 8. Overall system validation.

Input Values							
Fuel cell active area, A_{cell}	$135\,cm^2$		Number of cells	65		Methane Input, LHV_{CH4}	$1500\,W$
Results							
Electrical Power Output, $\dot{W}_{net}$			Net Electrical Efficiency			Total System Efficiency	
Korsgaard, 2008	$666\,W$		Korsgaard, 2008	0.45		Korsgaard, 2008	0.88
Arsalis, 2010	$669\,W$		Arsalis, 2010	0.4455		Arsalis, 2010	0.95

3.2 Full-load & Part-load Operation

The results for all the nodes, shown in Figure 1, are given in this section with the following parameters: temperature, mass flow rate, and mole fractions. In Table 9, the results for the full-load operation are given. In Tables 10, 11 and 12, the results for 75%, 50% and 25% load operation are given, respectively.

The current density variation for the given loads is shown in Figure 4, while the HT-PEMFC stack efficiency (LHV) variation for the given loads is given in Figure 5. The net electrical power output at full-load and part-loads vs. the corresponding cogeneration heat loads is shown in Figure 6.

Finally, the mass flow variation of hydrogen, methane, and carbon monoxide throughout the proposed micro-CHP system is shown in Figure 7. Mole fractions have not been used (although it could be done with mole fractions at dry basis), because it would appear as if the H_2 content has decreased at the exit of the WGS Reactor. This is because of the water addition at the reactor's inlet, which alters the total mass flow rate (and therefore the mole fractions) exiting the WGS Reactor.

Table 9. Results for nominal (full) load operation.

Node	$T(^{\circ}C)$	$\dot{m}\left(\frac{kg}{s}\right)$	X_{CH_4}	X_{CO}	X_{CO_2}	X_{O_2}	X_{N_2}	X_{air}	X_{H_2O}	X_{H_2}
1	10	5.53E-5	1	0	0	0	0	0	0	0
2	10	0	1	0	0	0	0	0	0	0
3	10	5.53E-5	1	0	0	0	0	0	0	0
4	200	5.53E-5	1	0	0	0	0	0	0	0
5	200	5.53E-5	1	0	0	0	0	0	0	0
6	200	2.5866E-4	0.229463	0	0	0	0	0	0.770537	0
7	602.507	2.5866E-4	0.0305163	0.0479166	0.0884621	0	0	0	0.335574	0.497558
8	250	2.5866E-4	0.0305163	0.0479166	0.0884621	0	0	0	0.335574	0.497558
9	296.621	3.25915E-4	0.0257661	0.00327824	0.111872	0	0	0	0.401797	0.457287
10	160	3.25915E-4	0.0257661	0.00327824	0.111872	0	0	0	0.401797	0.457287
11	160	1.52287E-4	0.0430648	0.0054802	0.187014	0	0	0	0	0.764441
12	160	4.56862E-5	0.0430648	0.0054802	0.187014	0	0	0	0	0.764441
13	10	4.76799E-3	0	0	0	0	0	1	0	0
14	10	4.76799E-3	0	0	0	0	0	1	0	0
15	33.1717	4.76799E-3	0	0	0	0	0	1	0	0
16	85.2871	4.76799E-3	0	0	0	0	0	1	0	0
17	820	4.84106E-3	0	0.000139963	0.00586232	0.194702	0.777381	0	0.0219143	0
18	698.341	4.84106E-3	0	0.000139963	0.00586232	0.194702	0.777381	0	0.0219143	0
19	597.234	4.84106E-3	0	0.000139963	0.00586232	0.194702	0.777381	0	0.0219143	0
20	592.509	4.84106E-3	0	0.000139963	0.00586232	0.194702	0.777381	0	0.0219143	0
21	469.388	4.84106E-3	0	0.000139963	0.00586232	0.194702	0.777381	0	0.0219143	0
22	313.613	4.84106E-3	0	0.000139963	0.00586232	0.194702	0.777381	0	0.0219143	0
23	10	4.87062E-3	0	0	0	0	0	0	1	0
24	10	2.0336E-4	0	0	0	0	0	0	1	0
25	200	2.0336E-4	0	0	0	0	0	0	1	0
26	10	6E-4	0	0	0	0	0	0	1	0
27	60	6E-4	0	0	0	0	0	0	1	0
28	10	6.72551E-5	0	0	0	0	0	0	1	0
29	10	4E-3	0	0	0	0	0	0	1	0
30	60	4E-3	0	0	0	0	0	0	1	0
31	39.7/60	8E-3	0	0	0	0	0	0	1	0
32	160	1.69539E-3	0.00705773	0.000898129	0.0306491	0	0	0.808997	0.152398	0
33	90.8106	1.69539E-3	0.00705773	0.000898129	0.0306491	0	0	0.808997	0.152398	0

Table 10. Results for 75% load operation.

Node	$T(^{\circ}C)$	$\dot{m}\left(\frac{kg}{s}\right)$	X_{CH_4}	X_{CO}	X_{CO_2}	X_{O_2}	X_{N_2}	X_{air}	X_{H_2O}	X_{H_2}
1	10	3.44E-5	1	0	0	0	0	0	0	0
2	10	0	1	0	0	0	0	0	0	0
3	10	3.44E-5	1	0	0	0	0	0	0	0
4	200	3.44E-5	1	0	0	0	0	0	0	0
5	200	3.44E-5	1	0	0	0	0	0	0	0
6	200	1.60903E-4	0.229463	0	0	0	0	0	0.770537	0
7	677.16	1.60903E-4	0.00683928	0.0759256	0.0766893	0	0	0	0.306115	0.534472
8	250	1.60903E-4	0.00683928	0.0759256	0.0766893	0	0	0	0.306115	0.534472
9	323.881	2.04693E-4	0.0057746	0.00640613	0.122451	0	0	0	0.356398	0.50897
10	160	2.04693E-4	0.0057746	0.00640613	0.122451	0	0	0	0.356398	0.50897
11	160	1.04414E-4	0.00897066	0.00995357	0.190259	0	0	0	0	0.790817
12	160	3.13243E-5	0.00897066	0.00995357	0.190259	0	0	0	0	0.790817
13	10	3.53781E-3	0	0	0	0	0	1	0	0
14	10	3.53781E-3	0	0	0	0	0	1	0	0
15	34.1452	3.53781E-3	0	0	0	0	0	1	0	0
16	88.263	3.53781E-3	0	0	0	0	0	1	0	0
17	718	3.58913E-3	0	0.000252865	0.00478593	0.196939	0.778266	0	0.0197568	0
18	678.214	3.58913E-3	0	0.000252865	0.00478593	0.196939	0.778266	0	0.0197568	0
19	592.973	3.58913E-3	0	0.000252865	0.00478593	0.196939	0.778266	0	0.0197568	0
20	588.999	3.58913E-3	0	0.000252865	0.00478593	0.196939	0.778266	0	0.0197568	0
21	422.56	3.58913E-3	0	0.000252865	0.00478593	0.196939	0.778266	0	0.0197568	0

Node	T(°C)	ṁ (kg/s)	X_{CH_4}	X_{CO}	X_{CO_2}	X_{O_2}	X_{N_2}	X_{air}	X_{H_2O}	X_{H_2}
22	316.236	3.58913E-3	0	0.000252865	0.00478593	0.196939	0.778266	0	0.0197568	0
23	10	1.17029E-3	0	0	0	0	0	0	1	0
24	10	1.26503E-4	0	0	0	0	0	0	1	0
25	200	1.26503E-4	0	0	0	0	0	0	1	0
26	10	4E-4	0	0	0	0	0	0	1	0
27	60	4E-4	0	0	0	0	0	0	1	0
28	10	4.37899E-5	0	0	0	0	0	0	1	0
29	10	2E-3	0	0	0	0	0	0	1	0
30	60	2E-3	0	0	0	0	0	0	1	0
31	39.7/60	8E-3	0	0	0	0	0	0	1	0
32	160	1.22449E-3	0.00142894	0.00158551	0.0303066	0	0	0.813443	0.153236	0
33	63.9818	1.22449E-3	0.00142894	0.00158551	0.0303066	0	0	0.813443	0.153236	0

Table 11. Results for 50% load operation.

Node	T(°C)	ṁ (kg/s)	X_{CH_4}	X_{CO}	X_{CO_2}	X_{O_2}	X_{N_2}	X_{air}	X_{H_2O}	X_{H_2}
1	10	2.73E-5	1	0	0	0	0	0	0	0
2	10	0	1	0	0	0	0	0	0	0
3	10	2.73E-5	1	0	0	0	0	0	0	0
4	200	2.73E-5	1	0	0	0	0	0	0	0
5	200	2.73E-5	1	0	0	0	0	0	0	0
6	200	1.27693E-4	0.229463	0	0	0	0	0	0.770537	0
7	588.301	1.27693E-4	0.0412854	0.0412682	0.0877433	0	0	0	0.355064	0.474694
8	250	1.27693E-4	0.0412854	0.0412682	0.0877433	0	0	0	0.355064	0.474694
9	290.156	1.60233E-4	0.034858	0.00256511	0.106362	0	0	0	0.423144	0.433072
10	160	1.60233E-4	0.034858	0.00256511	0.106362	0	0	0	0.423144	0.433072
11	160	7.17623E-5	0.0604169	0.00444675	0.184384	0	0	0	0	0.750753
12	160	2.15287E-5	0.0604169	0.00444675	0.184384	0	0	0	0	0.750753
13	10	3.31423E-3	0	0	0	0	0	1	0	0
14	10	3.31423E-3	0	0	0	0	0	1	0	0
15	25.4425	3.31423E-3	0	0	0	0	0	1	0	0
16	60.6438	3.31423E-3	0	0	0	0	0	1	0	0
17	610	3.34462E-3	0	8.50443E-5	0.00421257	0.199166	0.781225	0	0.0153115	0
18	588.564	3.34462E-3	0	8.50443E-5	0.00421257	0.199166	0.781225	0	0.0153115	0
19	514.464	3.34462E-3	0	8.50443E-5	0.00421257	0.199166	0.781225	0	0.0153115	0
20	511.012	3.34462E-3	0	8.50443E-5	0.00421257	0.199166	0.781225	0	0.0153115	0
21	328.864	3.34462E-3	0	8.50443E-5	0.00421257	0.199166	0.781225	0	0.0153115	0
22	95.2573	3.34462E-3	0	8.50443E-5	0.00421257	0.199166	0.781225	0	0.0153115	0
23	10	4.73293E-3	0	0	0	0	0	0	1	0
24	10	1.00393E-4	0	0	0	0	0	0	1	0
25	200	1.00393E-4	0	0	0	0	0	0	1	0
26	10	2.6E-4	0	0	0	0	0	0	1	0
27	60	2.6E-4	0	0	0	0	0	0	1	0
28	10	3.25396E-5	0	0	0	0	0	0	1	0
29	10	1.8E-3	0	0	0	0	0	0	1	0
30	60	1.8E-3	0	0	0	0	0	0	1	0
31	39.7/60	4E-3	0	0	0	0	0	0	1	0
32	160	7.78238E-4	0.010052	0.000739838	0.0306772	0	0	0.806587	0.151944	0
33	9.45718	7.78238E-4	0.010052	0.000739838	0.0306772	0	0	0.806587	0.151944	0

Table 12. Results for 25% load operation.

Node	T(°C)	ṁ (kg/s)	X_{CH_4}	X_{CO}	X_{CO_2}	X_{O_2}	X_{N_2}	X_{air}	X_{H_2O}	X_{H_2}
1	10	1.35E-5	1	0	0	0	0	0	0	0
2	10	0	1	0	0	0	0	0	0	0
3	10	1.35E-5	1	0	0	0	0	0	0	0
4	200	1.35E-5	1	0	0	0	0	0	0	0
5	200	1.35E-5	1	0	0	0	0	0	0	0
6	200	6.31449E-5	0.229463	0	0	0	0	0	0	0.770537
7	577.567	6.31449E-5	0.0479855	0.0364961	0.0879519	0	0	0	0.366555	0.461125

8	250	6.31449E-5	0.0479855	0.0364961	0.0879519	0	0	0	0.366555	0.461125
9	285.462	7.90376E-5	0.0405131	0.00217432	0.102894	0	0	0	0.436462	0.417956
10	160	7.90376E-5	0.0405131	0.00217432	0.102894	0	0	0	0.436462	0.417956
11	160	3.44656E-5	0.0718781	0.0038584	0.182589	0	0	0	0	0.741675
12	160	1.03397E-5	0.0718781	0.0038584	0.182589	0	0	0	0	0.741675
13	10	1.70821E-3	0	0	0	0	0	1	0	0
14	10	1.70821E-3	0	0	0	0	0	1	0	0
15	24.1477	1.70821E-3	0	0	0	0	0	1	0	0
16	56.6516	1.70821E-3	0	0	0	0	0	1	0	0
17	585	1.72204E-3	0	6.6806E-5	0.00406236	0.199663	0.781831	0	0.0143764	0
18	577.567	1.72204E-3	0	6.6806E-5	0.00406236	0.199663	0.781831	0	0.0143764	0
19	506.196	1.72204E-3	0	6.6806E-5	0.00406236	0.199663	0.781831	0	0.0143764	0
20	502.873	1.72204E-3	0	6.6806E-5	0.00406236	0.199663	0.781831	0	0.0143764	0
21	148.251	1.72204E-3	0	6.6806E-5	0.00406236	0.199663	0.781831	0	0.0143764	0
22	93.2573	1.72204E-3	0	6.6806E-5	0.00406236	0.199663	0.781831	0	0.0143764	0
23	10	4.66554E-3	0	0	0	0	0	0	1	0
24	10	4.96449E-5	0	0	0	0	0	0	1	0
25	200	4.96449E-5	0	0	0	0	0	0	1	0
26	10	1.3E-4	0	0	0	0	0	0	1	0
27	60	1.3E-4	0	0	0	0	0	0	1	0
28	10	1.58927E-5	0	0	0	0	0	0	1	0
29	10	9E-4	0	0	0	0	0	0	1	0
30	60	9E-4	0	0	0	0	0	0	1	0
31	39.7/60	2E-3	0	0	0	0	0	0	1	0
32	160	3.67297E-4	0.0120806	0.000648486	0.0306879	0	0	0.804948	0.151635	0
33	90.9467	3.67297E-4	0.0120806	0.000648486	0.0306879	0	0	0.804948	0.151635	0
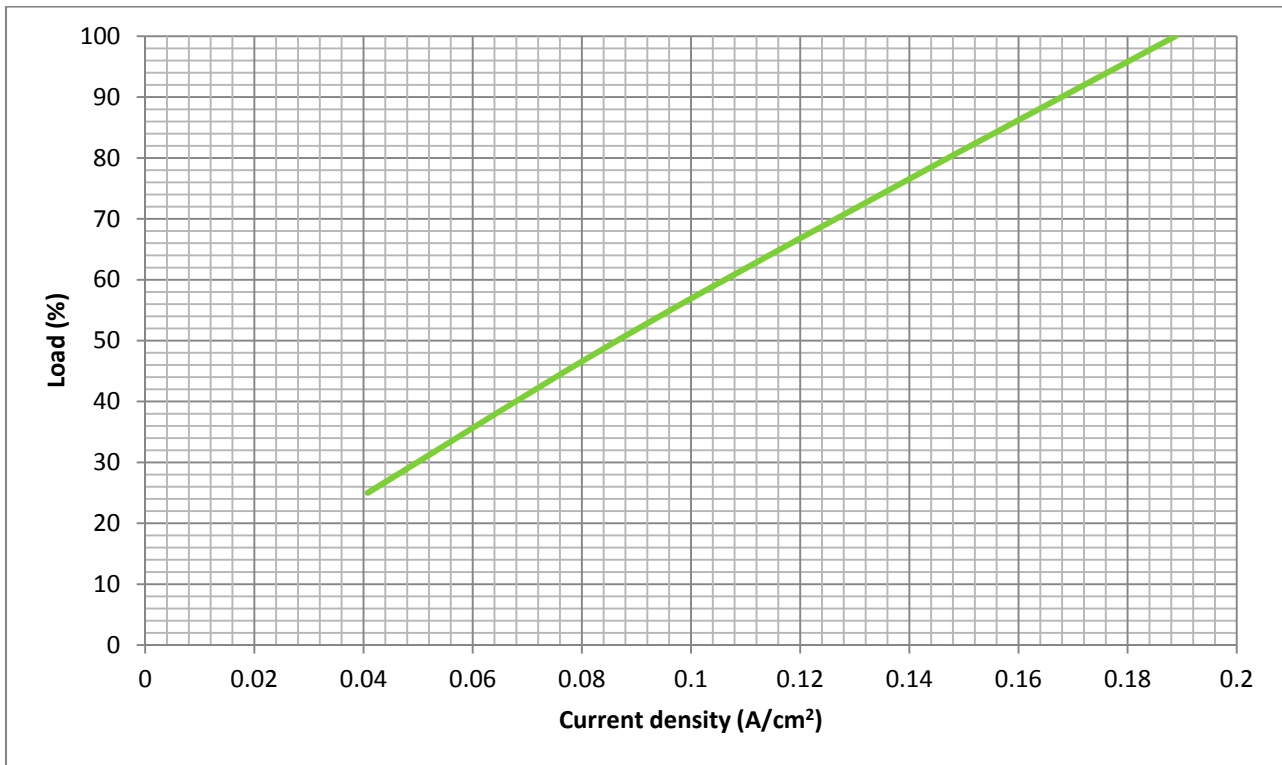
Figure 4. Current density vs. Load.
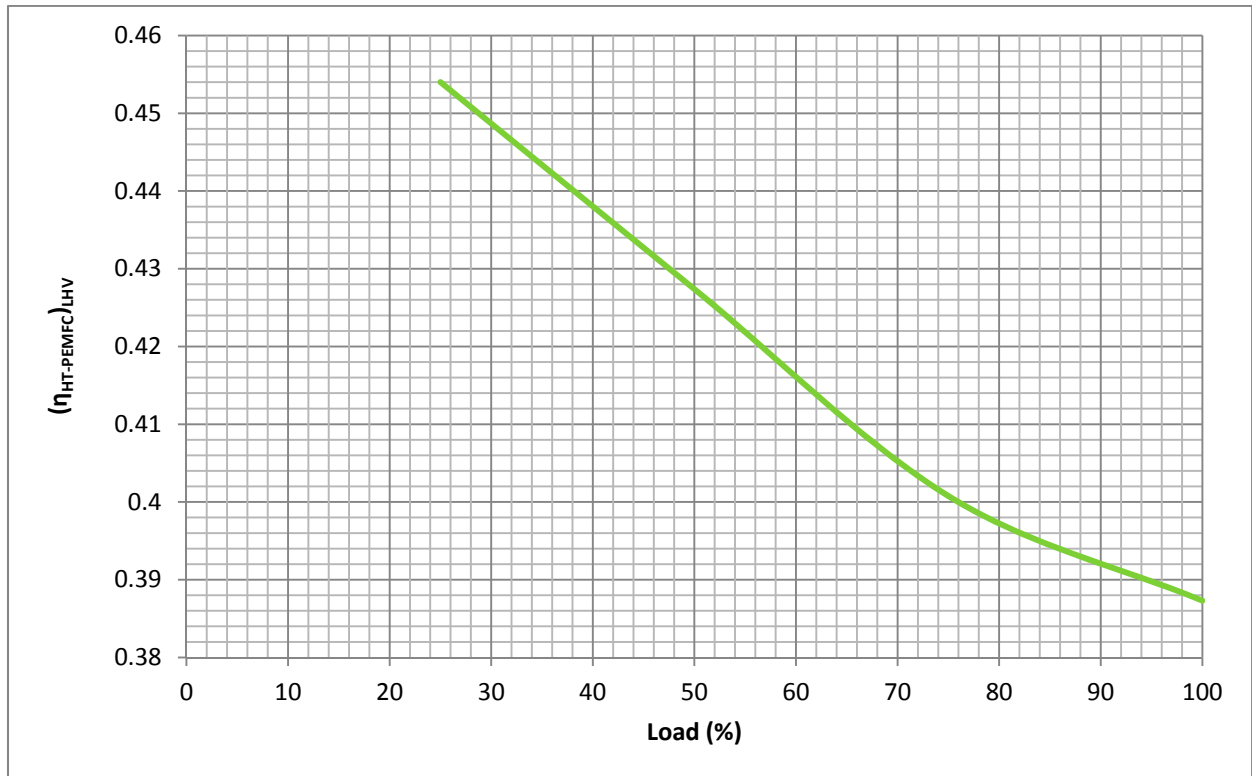
Figure 5. HT-PEMFC efficiency vs. Load.
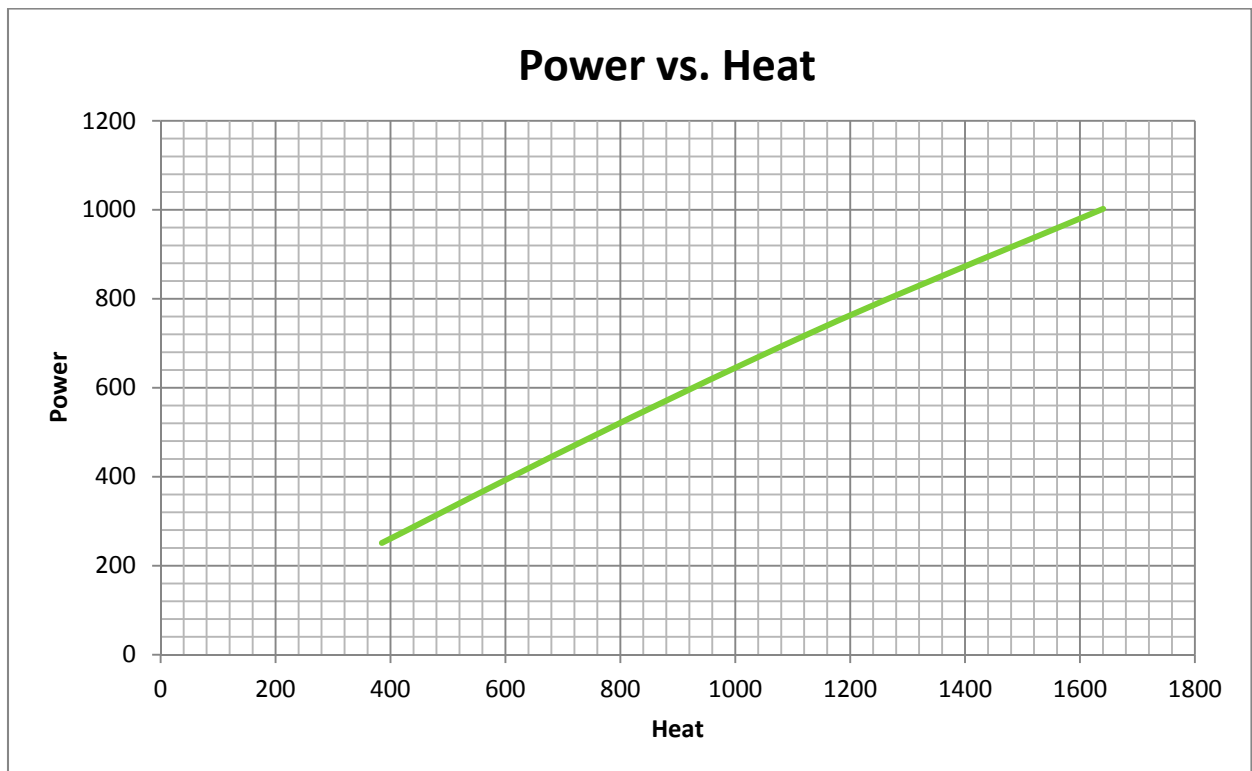
Figure 6. Electrical Load vs. Total Cogeneration Heat Load.
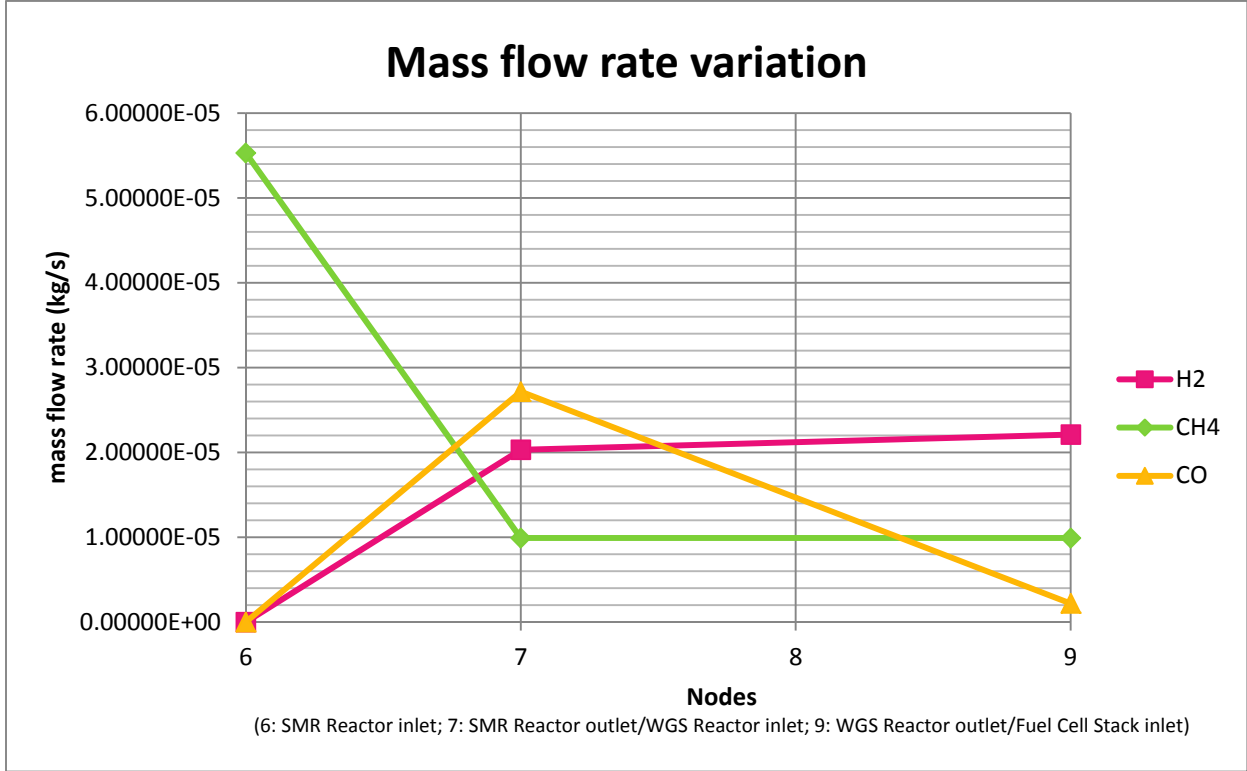
Figure 7. Mass flow variation of hydrogen, methane and carbon monoxide in the proposed micro-CHP system.

3.3 Analysis of Cogeneration Results

The system's useful heat capacity was analyzed in section 2.10.4. For the load profile, defined in 1.4, the net electrical power output, along with the corresponding total cogeneration heat output are given in Table 13. In the same table, the percentage of heat output fulfilling the aforementioned load profile at every time segment is also given.

Table 13. Overall performance of the proposed micro-CHP system.

Load	$\left(\dot{W}_{electrical}\right)_{net}(W)$	$\left(\dot{Q}_{HEx}\right)_{cogen.}(W)$	Total Cogeneration Heat Load fulfilled (%)
Winter, mean	540	840	47.2%
Winter, max	950	1560	51.8%
Summer, mean	380	580	193%
Summer, max	650	1000	64.1%
Spring, mean	460	700	76.9%
Spring, max	920	1470	54.6%

3.4 Component Geometries

The HT-PEMFC stack, SMR reactor and the WGS reactor geometries for the proposed micro-CHP system are given in Table 14. The UA-values for the heat exchangers used in the proposed micro-CHP system are given in Table 15.

Table 14. Component geometries for the proposed micro-CHP system.

	Geometric Variable Description	Value			Geometric Variable Description	Value
n_{cells}	Number of Cells	176		L^{SMR}	SMR Tube Length	0.8 m
D_i^{SMR}	SMR Inlet Tube Diameter	0.1016 m		D_i^{WGS}	WGS Tube Diameter	0.13 m
D_o^{SMR}	SMR Outlet Tube Diameter	0.1322 m		L^{WGS}	WGS Tube Length	0.45 m

Table 15. UA-values [W/(m^2-$^{\circ}$C)] for the heat exchangers used in the proposed micro-CHP system.

	Geometric Variable Description	Value			Geometric Variable Description	Value
UA_I	Natural Gas Preheater	0.0538784		UA_{IV}	1st Cogeneration Heat Exchanger	1.41641
UA_{II}	SMR/WGS Cooler	0.720725		UA_V	2nd Cogeneration Heat Exchanger	2.36245
UA_{III}	WGS/HT-PEMFC Cooler	0.548661		UA_{VI}	3rd Cogeneration Heat Exchanger	1.39233
$UA_{SG,sup}$	Superheater (Steam Generator)	0.107073		$UA_{SG,ec}$	Economizer (Steam Generator)	0.0896212
$UA_{SG,ev}$	Evaporator (Steam Generator)	0.843147				

3.5 Discussion

As expected the combined heat load is satisfied better in the summer segment. It should be noted that there would still be a deficit of heat at some instances in the summer if no heat storage is provided. In the case of the other two time segments, winter and spring, an auxiliary burner will be required at some instances, even if a heat storage system is used. More specifically for the winter segment, the heat load can be fulfilled at around 50% in most instances.

The HT-PEMFC stack is assumed to withstand CO-contents in the inlet reforming fuel of up to 10,000ppm. The CO-content was maintained within this limit and was calculated to be 5480ppm. This result verifies that the current design of the fuel processing system, although simple, it can be adequate for the needs of the fuel cell stack, at least in terms of CO-content removal.

The electrical power output is controlled by regulating the incoming natural gas amount to the fuel processing subsystem. The current density was tested at part-load to drop up to 0.04 A/cm2. In a realistic fuel cell stack it should be investigated at up to which level the current density can be reduced. Although experimental results indicated a high level of tolerance for HT-PEMFC stacks at load variations, rapid and frequent load changes might shorten the fuel cell stack's lifetime.

4   Conclusions

The proposed micro-CHP system combines the high electrical efficiency potential of HT-PEMFC technology, with a complete, yet simplified, fuel processing subsystem: The result is a realistic compact micro-CHP system which can provide a basis for further experimental and data acquisition testing in the developing process of the end-user (commercial) product.

As explained the target of this study was to investigate the modeling capabilities of a system designed in LabVIEW at steady-state operation. An averaged load profile adjusted for three time segments of the year was tested at full-load and part-load operation. An electrical efficiency varying from 45.4% (25%- load) to 38.8% (full-load) was calculated. The corresponding total efficiency was around 95.2%.

One of the most important advantages of the proposed system is the simplicity of the fuel processing system. It should be noted that simplicity is necessary, because the micro-CHP system must maintain a high level of compactness. The fuel processing system provides a high degree of methane conversion and acceptable CO-removal, making it appropriate for integration with an HT-PEMFC stack. Inaccuracies were inevitable, especially in the fuel processing system, due to the lack of matching semi-empirical functions, which are due in the future, for small scale fuel processing systems. The modeling used in the SMR and WGS reactors is based on reaction kinetics, which provide more realistic results and also it can be easy to adjust the modeling when new experimental kinetic data become available.

Further on, the obtained efficiencies for the proposed system, verified the great potential of the HT-PEMFC technology in micro-CHP systems. A lot of ground for improvement is necessary before the end-user system is available; the modeling results have to be verified by experimental testing to investigate sources of discrepancy and other hurdles, such as incompatibility of the subsystems. Also, more appropriate experimental assumptions than those used in the current study are necessary as explained in the preceding chapter.

Finally, LabVIEW was chosen as the modeling tool for this research study for the reasons explained in the introduction. Although the end result can provide a high degree of easiness to the program user in terms of calculations, the modeling procedure proved to be very time-consuming. There is a great difficulty in adjusting and modifying highly complicated models, due to the graphical modeling nature used in LabVIEW. Also LabVIEW has a limited number of parameters that can be transferred from subVI[2] to subVI. Therefore, LabVIEW modeling is more appropriate for single component dynamic systems. Nonetheless, the current system can provide a good tool for experimental testing in the future.

---

[2] A subVI is the LabVIEW equivalent to "functions," "subroutines," and "methods" in other programming languages.

References

de Wit, J. (2006). Implementation of micro CHP in Single-family Houses. *23rd World Gas Conference.* Amsterdam, The Netherlands.

Georgopoulos, N. G. (2002). *Application of a Decomposition Strategy to the Optimal Synthesis/Design and Operation of a Fuel Cell Based Total Energy System.* MS Thesis: Virginia Tech, Blacksburg, VA, USA.

Keiski, R., Salmi, T., Niemisto, P., Ainassaari, J., & Pohjola, V. (1996). Stationary and transient kinetics of the high temperature water-gas shift reaction. *Applied Catalysis A: General* , 349-370.

Kim, K. (2008). *Dynamic Proton Exchange Membrane Fuel Cell System Synthesis/Design and Operation/Control Optimization under Uncertainty.* PhD Dissertation: Virginia Tech, Blacksburg, VA, USA.

Korsgaard, A. R., Nielsen, M. P., & Kær, S. K. (2008). Part one: A novel model of HTPEM-based micro-combined heat and power fuel cell system. *I. J. of Hyrdogen Energy* , 1909-1920.

Li, C., & Finlayson, B. (1977). Heat Transfer in Packed Beds-A Reevaluation. *Chemical Engineering Science* , 1055-1066.

micro-CHP, D. (2010, 4 23). Retrieved 4 23, 2010, from http://www.dk-mchp.eu

Nielsen, M. P. (2005). *Modeling of Proton Membrane Fuel Cell Systems.* Aalborg: Aalborg University.

Pedersen, A. H., & Balslev, P. (2009). Demonstration of μCHP Based on Danish Fuel Cells (Phase 1+ first part of Phase 2). *European Fuel Cell Forum 2009*, (pp. 1-7). Lucerne, Switzerland.

Xu, J., & Froment, G. (1989). Methane Steam Reforming, Methanation and Water-Gas Shift: 1. Intrinsic Kinetics. *AIChE Journal* , 88-96.

Zhang, J., & Xie, Z. (2006). High temperature PEM fuel cells. *J. Power Sources , 160*, 872-891.

Appendix

In the appendix, LabVIEW screenshots are shown to illustrate the modeling structure and parameter calculation for the overall system (VI) and the main subsystems (subVIs). In Figure 8, the Overall System (main) VI is shown, while in Figures 9-13 the Combustor, Fuel Cell Stack, Steam Generator, SMR and WGS Reactors subVIs are shown, respectively.

Figure 8. LabVIEW front panel of the HT-PEMFC-based micro-CHP system.

COMBUSTOR

Inlet

Depleted fuel from fuel cell stack anode

Temperature

T_fc

| 160 | degC

Mass flow rate

m_dot_df_total

| 1.06958E-4 | kg/s

Mole Fractions

x_H2_fuel_in

| 0.570027

x_CH4_fuel_in

| 0.00695971

x_CO_fuel_in

| 0.00495167

x_CO2_fuel_in

| 0.273769

Air needed for combustion (from HEx between SMR & WGS Reactors)

Temperature

T_air

| 327 | degC

Mass flow rate

m_dot_air

| 4.45303E-3 | kg/s

Total mass flow rate at inlet

m_dot_total_i

| 4.55999E-3 | kg/s

Outlet

Flue gas to SMR reactor's shell-side

Temperature

T_fg

| 826.85 | degC

Mole Fractions

x_H2O_out

| 0.0225974

x_CO2_out

| 0.0107413

x_CO_out

| 0.000189461

x_N2_out

| 0

x_O2_out

| 0.192745

Total mass flow rate at outlet

m_dot_total_o

| 4.59138E-3 | kg/s

Balanced reactions for the selected operating conditions

nu_O2_f1

$H2 + \boxed{8.90073} (O2+3.76N2) \longrightarrow H2O + nu\_O2\_f1(3.76)N2 + (nu\_O2\_f1-0.5)O2$

nu_O2_f2

$CH4 + \boxed{29.7301} (O2+3.76N2) \longrightarrow CO2 + 2H2O + nu\_O2\_f2(3.76)N2 + (nu\_O2\_f2-2)O2$

Molal Analysis

Total mols at exit

n_total_f1   n_total_f2

| 42.8675 | | 142.515 |

Mass defect (mass balance)

mass_defect

| 3.13937E-5 | kg/s

Assumptions:
(1) Combustion of CH4/H₂ with O₂ is based on problem 14.52, Sonntag, Thermodynamics.
(2) The temperature of the products (= T flue gas) is regulated to remain constant.
(3) No additional CH₄ from the line is considered.

Figure 9. LabVIEW front panel of the Combustor subVI.

FUEL CELL STACK

OPERATIONAL CONDITIONS

Cell Total pressure
p
1 bar

Cell Temperature
T
160 degC

Stoichiometry
Cathode
lambda_air
2.7
Anode
lambda_H2
1.3

Current density
(at given stack load,
variable @part-load)
i
0.2 A/cm^2

AMBIENT CONDITIONS

Ambient relative humidity
r_ambient
0.7
Ambient temperature
T_ambient
20 degC

STACK DESIGN
Number of cells
n_cells
176

Active MEA area in cells
A_cell
49 cm^2

KINETIC MODEL RATES
++They account for temp. variations
using Arrhenius-type expressions
++These constants are used to
calculate the anode overpotential
due to CO-poisoning

desorption rate
b_fc
CO 0.00369534 bar
b_fh
H2 3.40512 bar

electrooxidation rate
k_ec
CO 5.98675E-6 A/cm^2
k_eh
H2 1.63818 A/cm^2

adsorption rate
k_fc
CO 0.47504 A/cm^2 bar
k_fh
H2 34.4258 A/cm^2 bar

PARAMETER REGRESSIONS FOR CATHODE
AND OHMIC CELL LOSSES AS FUNCTION
OF CELL TEMPERATURE

Open circuit voltage
V_0
0.95 V

Exchange current density
i_0
2.01926E-4 A/cm^2

alpha_anode alpha_cathode
0.5 0.250709

R_ohmic R_diff
0.156667 Ohm cm^2 0.075286 Ohm cm^2

(see subVI: thetas_evaluation.vi)

CO & H2 SURFACE COVERAGE BASED ON
STEADY-STATE KINETIC BALANCES
Balances=0 @ steady-state conditions otherwise
they equal coverage time differentials

2nd order kinetics assumed with respect to
H2 coverage
n
2

H2 adsorption minus desorption ~ current density
@ steady-state

theta_H2
0.142115

CO adsorption minus desorption corrected
for electro-oxidation ratio should balance
theta_CO
0.523281

OVERPOTENTIALS

Anode overpotential
(assuming alpha=0.5 in the simplified
Butler-Volmer equation)
eta_a
0.0311518 V

Cathode overpotential
(function developed by Anders Korsgaard
based on measurements)
eta_c
0.265634 V

Ohmic overpotential
(mainly losses due to proton conduction
in E-cat and electrolyte)
eta_ohmic
0.0313333 V

Total Cell Voltage (modeled)
V_cell
0.621881 V

BALANCE OF FUEL CELL STACK

Power Density W_cell
0.124376 W/m^2

Stack Voltage V_stack
109.451 V

Stack Power P_stack
1072.62 W

Stack Current I_stack
9.80001 A

Electrical Efficiencies
eta_el_LHV eta_el_HHV
0.382023 0.322709

Theoretical Voltage E_th
1.26006 V
P_th
Power Losses 1100.74 W

Reformate Fuel IN (anode gas)

(input from the WGS, water content removed
in the knock-out stage prior to FC input)
1.53574E-5 [kg/s] *Mole Fractions*
@ full-load
m_dot_fuel_in_H2 x_H2_fuel_in
2.34252E-5 kg/s 0.666147

m_dot_fuel_in_CH4 x_CH4_fuel_in
2.27601E-6 kg/s 0.00813328

m_dot_fuel_in_CO x_CO_fuel_in (10000e-6
2.82724E-6 kg/s 0.00578664 =10000ppm
=1% CO)
m_dot_fuel_in_CO2 x_CO2_fuel_in
2.45603E-4 kg/s 0.319933
m_dot_fuel_in_total
2.74131E-4 kg/s

Depleted Reformate Fuel (to combustor)
m_dot_df_H2
7.02756E-6 kg/s
m_dot_df_CH4
6.82803E-7 kg/s

m_dot_df_CO
8.48172E-7 kg/s
m_dot_df_CO2
7.36809E-5 kg/s

m_dot_df_total
8.22394E-5 kg/s

Cathode

Total Air in m_dot_air_in
1.66461E-3 kg/s

O2 consumed m_dot_O2_used
by the fuel cell 1.43011E-4 kg/s

Total air m_dot_air_out
exhausted from 1.5216E-3 kg/s
the cathode

Water in m_dot_H2O_ambient
ambient air 1.72287E-5 kg/s

Anode
Total water m_dot_exit_total_anode
mixture 3.53789E-4 kg/s
exhausted from
the anode

Total mixture exhausted
from the fuel cell stack
m_dot_exit_total
1.87539E-3 kg/s

Mole Fractions

x_CO2_exit
0.0587487

x_CO_exit
0.00106259

x_H2O_exit
0.1488

x_CH4_exit
0.0014935

x_air_exit
0.789896

Model Validation

Mass Defect
1.6575E-6 kg/s

Figure 10. LabVIEW front panel of the Fuel Cell Stack subVI.

STEAM GENERATOR

Temperatures

T_h_A
754.648 degC

T_h_B
732.939 degC

T_h_C
586.218 degC

T_h_D
572.979 degC

T_c_1
20 degC

T_c_2
100 degC

T_c_3
100 degC

T_c_4
200 degC

Pressures

p_h
1.1 bar

p_c = 1.1 bar

Mass flow rates

m_dot_h
4.59138E-3 kg/s

m_dot_c
3.49499E-4 kg/s

take this value as an input
from the NG preheater subvi

Mole fractions

x_H2O_v_h
0.0225974

x_CO2_h
0.0107413

x_CO_h
0.000189461

x_N2_h
0.773727

x_O2_h
0.192745

Specific Heats

C_p_h_A
1175.11 J/kg K

C_p_h_B
1170.93 J/kg K

C_p_h_C
1138.39 J/kg K

Heat transfer rate

Q_dot_sup
117.127 W

Q_dot_eva
788.797 W

Q_dot_eco
69.2008 W

UA-value

UA_sup
0.171393 W/m^2 degC

UA_eva
1.41779 W/m^2 degC

UA_eco
0.161633 W/m^2 degC

Hot flue gas
(from SMR exhaust)

C

economizer   evaporator   superheater   A

Subcooled water
(from water pump)

Saturated water   Saturated vapor   Superheater Steam
(to CH4-steam
Mixer)

1   2   3   4

D   B

Cooled flue gas
(to Fuel Preheater HEx)

Working mediums
hot-side: flue gas from SMR exit (shell-side) to fuel preheater inlet (plate HEx)
cold-side: water from the water pump/by-pass valve exit to CH4-steam mixer

based on a plate heat exchanger model

Figure 11. LabVIEW front panel of the Steam Generator subVI.

STEAM METHANE REFORMER

SMR Geometry

Tube diameters

D_i
0.1016 m

D_o
0.1322 m

Tube length

L_tube
0.8 m

Tube-side (reformate)

Initial length
z initial
0 m

Final length (just to check)
z final
0.8 m

Total Discretization steps
steps
300

Discretization step length
dz
0.00266667 m

Extent of reaction

in | out
X CH4, in | X CH4, out
0 | 0.961105

X CO2, in | X CO2, out
0 | 0.480573

Temperature

Reformate | Inside wall
T ref, i | T_wall_i, i
200 degC | 327 degC

T ref, o | T_wall_i, o
679.854 degC | 709.049 degC

Pressure

p initial
1.1 bar

p final
1.08875 bar

Inlet Feed Rates
kg/s | *Mole fractions*

m_dot_CH4_in | x_CH4_in
9.357E-5 kg/s | 0.229463
must be an input from
the NG preheater subVI

m_dot_H2O_in | x_H2O_in
3.44094E-4 kg/s | 0.770537

m_dot_total_in
4.37664E-4 kg/s

Outlet flow rates
kg/s | *Mole fractions*

m_dot_H2_out | x_H2_out
3.87975E-5 kg/s | 0.535886

m_dot_CH4_out | x_CH4_out
3.52212E-6 kg/s | 0.00611445

m_dot_CO2_out | x_CO2_out
1.21086E-4 kg/s | 0.076613

m_dot_H2O_out | x_H2O_out
1.97322E-4 kg/s | 0.304916

m_dot_CO_out | x_CO_out
7.69367E-5 kg/s | 0.0764857

m_dot_total_out
4.37664E-4 kg/s

Shell-side (flue gas)

Mass flow rate of the flue gas

m_dot_flue gas
4.59138E-3 kg/s (must be an input from the combustor model)

Temperature of the flue gas

T_fg, i
827 degC

T_fg, o
743.049 degC

Mole fractions

x_CO_fg
0.000189461

x_O2_fg
0.192745

x_H2O_fg
0.0225974

x_CO2_fg
0.0107413

x_N2_fg
0.773727

Hot flue gas (in) 19
CH4-steam mixture 21
Steam Methane Reformer
22 Reformate gas
20 Hot flue gas (out)

The reaction model is based on:
SteamReformer.EES,
SteamReformer.m
by Nielsen, 2005
(Xu & Froment, 1989)

The heat exchanger model is based on:
Kim, 2008

Figure 12. LabVIEW front panel of the SMR Reactor subVI.

Figure 13. LabVIEW front panel of the WGS Reactor subVI.